catalysts

MDPI

Article

Hydrodeoxygenation–Isomerization of Methyl Palmitate over SAPO-11-Supported Ni-Phosphide Catalysts

Ivan V. Shamanaev *, Irina A. Shamanaeva, Ekaterina V. Parkhomchuk and Galina A. Bukhtiyarova *

Boreskov Institute of Catalysis, Lavrentiev Ave. 5, 630090 Novosibirsk, Russia
* Correspondence: i.v.shamanaev@catalysis.ru (I.V.S.); gab@catalysis.ru (G.A.B.)

Abstract: Ni-phosphide catalysts on SAPO-11 were studied in the hydrodeoxygenation–isomerization of methyl palmitate ($C_{15}H_{31}COOCH_3$—MP). The catalysts were synthesized using temperature-programmed reduction (TPR) of a phosphate precursor ($(NH_4)_2HPO_4$ and $Ni(CH_3CH_2COO)_2$), TPR of a phosphite precursor (H_3PO_3 and $Ni(OH)_2$), and using phosphidation of Ni/SAPO-11 by PPh_3 in the liquid phase. The samples were characterized by ICP-AES chemical analysis, N_2 physisorption, NH_3-TPD, XRD, and TEM. First, the screening of the catalysts prepared by the TPR method was carried out in a semi-batch autoclave to determine the influence of the preparation method and conditions on one-pot HDO–isomerization (290–380 °C, 2–3 MPa). The precursor's nature and the amount of phosphorus strongly influenced the activity of the catalysts and their surface area and acidity. Isomerization occurred only at a low P content (Ni/P = 2/1) and blocking of the SAPO-11 channels by unreduced phosphates at higher P contents did not allow us to obtain iso-alkanes. Experiments with liquid phosphidation samples in a continuous-flow reactor also showed the strong dependence of activity on phosphidation duration as well as on Ni content. The highest yield of isomerized products (66% iso-$C_{15–16}$ hydrocarbons, at complete conversion of O-containing compounds, 340 °C, 2 MPa, and LHSV = 5.3 h^{-1}) was obtained over 7% Ni_2P/SAPO-11 prepared by the liquid phosphidation method.

Keywords: hydrodeoxygenation; isomerization; Ni-phosphide; SAPO-11; methyl palmitate; biofuel; green diesel

Citation: Shamanaev, I.V.; Shamanaeva, I.A.; Parkhomchuk, E.V.; Bukhtiyarova, G.A. Hydrodeoxygenation–Isomerization of Methyl Palmitate over SAPO-11-Supported Ni-Phosphide Catalysts. *Catalysts* **2022**, *12*, 1486. https://doi.org/10.3390/catal12111486

Academic Editors: Junjian Xie and Qiang Deng

Received: 28 October 2022
Accepted: 18 November 2022
Published: 21 November 2022

1. Introduction

Renewable sources have attracted much attention in the production of fuels and chemical products. Hydrodeoxygenation (HDO) of fatty-acid-based feedstocks (vegetable oils, animal fats, tall oils) leads to the formation of normal alkanes [1]. HDO is carried out over Ni(Co)Mo/Al_2O_3 catalysts, resulting in products with a high cetane index but poor low-temperature properties (high cloud and pour points) [2–4]. Isomerization of these products is needed to meet the requirements of commercial fuels. Noble metal catalysts on silicoaluminophosphates (SAPOs) or zeolites are used in these processes [5]. Overall, the process is two-step [6], and there is an attractive approach to combine HDO and isomerization into one step over bifunctional catalysts [7].

The most attractive SAPOs for different applications are SAPO-34 [8–10], SAPO-11 [11–15], SAPO-5 [16–18], SAPO-31 [19–21], and SAPO-41 [22–24]. SAPO-11 with the AEL topology is a member of the class of one-dimensional molecular sieves applied in hydroisomerization [25,26]. It possesses a medium-sized (0.4 × 0.65 nm) pore structure and mild acidity, which provides high selectivity in the hydroisomerization of n-alkanes [27,28].

New classes of catalysts based on transition metal carbides, nitrides, and phosphides are attracting a considerable amount of interest for application in hydroconversion reactions [29–32]. Due to their high activity, phosphides are particularly interesting for HDO [33–35]. Ni-phosphide catalysts are among the most active [36–39]. There are several works on bifunctional Ni-phosphide SAPO-11 catalysts for fatty acid ester HDO–isomerization and n-alkane isomerization.

Heng Shi et al. [40] prepared 15 wt.% Ni_2P/SAPO-11 with an initial Ni/P ratio of 1/1 by temperature-programmed reduction (TPR) of the phosphate precursor and tested it in methyl laurate ($C_{11}H_{23}COOCH_3$) hydroconversion. At 340 °C, 2 MPa, and WHSV = 10 h^{-1}, the methyl laurate conversion was 78% and the selectivity to $C_{11–12}$ was 92%, but only a small amount of hydroisomerization was achieved because a high Ni loading suppresses medium-strength acid sites [40,41].

Sha Zhao et al. [41] investigated the performance of 3 wt.% Ni_2P/SAPO-11 catalysts in HDO–isomerization of methyl laurate. The catalyst was prepared by TPR of the phosphate precursor (NiP = 1/1). At 360 °C, 3 MPa, and WHSV = 2 h^{-1}, the methyl laurate conversion was close to 100% and the selectivity to iso-alkanes (iso-$C_{11–12}$) decreased from ~37 to ~29% during 101 h of experimentation. The selectivity to $C_{6–10}$ cracked products was ~10%.

Liu Chun-ya et al. [42] carried out HDO–isomerization of a methyl oleate ($C_{17}H_{33}COOCH_3$) and methyl stearate ($C_{17}H_{35}COOCH_3$) mixture over NiP/SAPO-11 with different Ni contents (1–13 wt.%), prepared by TPR of the phosphate precursor with Ni/P = 1/1. The carrier was prepared by the extrusion method with pseudo-boehmite (SAPO-11: pseudo-boehmite = 7:3). The highest isomerization rate was observed for the catalyst with 3 wt.% of Ni. At 340 °C, 2 MPa, and WHSV = 2.5 h^{-1}, the methyl ester conversion was ~98% and the isomerization selectivity was 14% (iso-$C_{15–18}$).

Shasha Tian and Jixiang Chen [43] studied Ni_2P/SAPO-11 catalysts in n-dodecane isomerization. The catalysts were prepared by TPR of the phosphate precursor with different Ni/P ratios and Ni contents. The highest isododecane selectivity of 72% was achieved at 90% conversion over the 3% Ni_2P/SAPO-11 catalyst with Ni/P = 1/1 (at 350 °C, 2 MPa, and WHSV = 2 h^{-1}).

Siyang Liu et al. [44] studied HDO–hydrocracking of castor oil over SAPO-11-supported Ni, NiAg, and Ni_2P catalysts. The 25% Ni_2P/SAPO-11 was prepared by the hypophosphite decomposition method with an initial Ni/P ratio of 1/1.5. This catalyst did not show significant isomerization and hydrocracking activity. At 300 °C, 3 MPa, and WHSV = 2 h^{-1}, the iso/normal alkanes ratio ($C_{8–15}$) was 0.1, the yield of $C_{5–7}$ hydrocarbons was 5%, the yield of $C_{8–15}$ was 2%, and the yield of $C_{16–19}$ was 92% (at 99% conversion). Similar results were obtained for 25% Ni/SAPO-11. The iso/normal alkanes ratio was 0.1, and the yields were 1% for $C_{5–7}$, 3% for $C_{8–15}$, and 95% for $C_{16–19}$.

Hongbiao Tang et al. [45] used SAPO-11, Zr-SBA-15, and ZSM-5 for NiMoP catalyst synthesis by TPR of phosphate precursors. The Ni/Mo ratio was 1/1, the total metal content was 5 wt.%, and the metal-to-P ratio was set to 1/2, 1/1, 2/1, and 3/1. The catalysts were tested in jatropha oil conversion in an autoclave at 360 °C and 3 MPa for 4 h. The products were divided into four groups: naphthenes, aromatics, oxygenates, and $C_{8–16}$ alkanes. For SAPO-11-supported catalysts, the P content did not significantly influence the selectivity of the $C_{8–16}$ alkanes (47–50%). The highest content of naphthenes was achieved for the sample with Ni/P = 1/2 (21%). The lowest content of oxygenates was achieved for the sample with Ni/P = 3/1 (5%).

Yang Zhang et al. [46] prepared a 4 wt.% Ni_2P/SAPO-31 catalyst by TPR of the phosphate precursor for isomerization of n-hexadecane. The selectivity to isohexadecane was ~82% at 80% conversion (at 380 °C, 2 MPa, and WHSV = 3.7 h^{-1}).

Previous works on SAPO-supported Ni-phosphide catalysts have mainly focused on phosphate precursors. No direct comparison of the influence of the precursor's nature on the catalytic activity has been carried out. No one to the best of our knowledge has studied catalysts prepared by the liquid phosphidation method. However, this method may be advantageous for preventing the interaction of the P precursor with the support, which is well-known for Al_2O_3-supported catalysts [37,47–50].

The aim of this work is to study the influence of the preparation method on the catalytic activity of SAPO-11-supported Ni-phosphide catalysts in HDO–isomerization of methyl palmitate ($C_{15}H_{31}COOCH_3$) (MP). Our study involved the screening of the catalysts using an autoclave reactor to verify the activity of TPR catalysts and determine the conditions for optimal HDO–isomerization, the preparation and testing of liquid phosphidation catalysts

in a continuous-flow reactor and a comparison with TPR catalysts, and physicochemical analysis of the most promising catalysts.

2. Results and Discussion

2.1. Catalyst Screening

2.1.1. TPR Catalyst Screening and Search for Optimal Conditions in an Autoclave

The catalysts were prepared by incipient wetness impregnation of the support with two different precursors (phosphate and phosphite) with subsequent TPR. The samples were labeled NiP_A (phosphate) and NiP_I (phosphite).

SiO_2-supported NiP_I samples show higher activity in MP HDO than NiP_A samples [36]. Therefore, we started screening in an autoclave using NiP_I/SAPO-11 samples (7 wt.% of Ni). Figure 1 shows MP conversion (X_{MP}) and conversion of O-containing compounds (X_O) vs. time for NiP_I/SiO_2 and for three independently synthesized NiP_I/SAPO-11 catalysts. Surprisingly, the SAPO-11-supported samples did not have any HDO–isomerization activity. X_{MP} over NiP_I/SiO_2 (Ni_2P/SiO_2) reached 89% in 5 h. This demonstrates that the conditions are good for HDO.

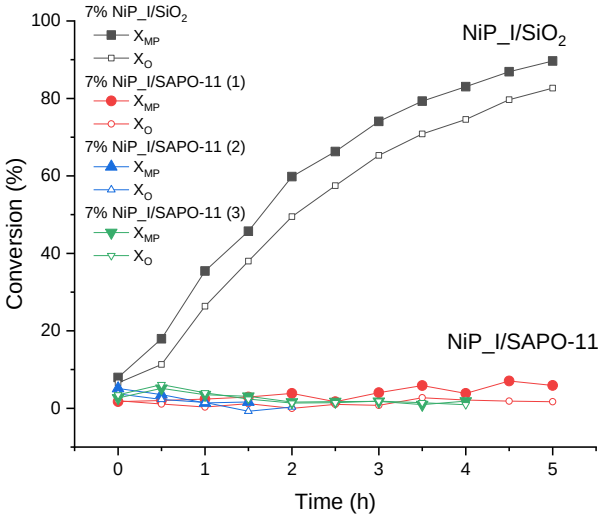

Figure 1. Conversion of MP and O-containing compounds over NiP_I/SiO_2 and NiP_I/SAPO-11 catalysts in an autoclave (290 °C, 3 MPa, V_{H2} = 100 mL/min, 500 RPM, m_{cat} = 1 g).

SAPO-11 is a microporous material (Table S1) and micropores as well as mesopores can be blocked by excess P. For example, it was shown that Ni/zeolite catalysts have a larger surface area than $Ni(H_2PO_4)_2$/zeolite catalysts [51]. Indeed, S_{BET} significantly decreased after phosphide preparation (29 m^2/g, Table S1) and after reaction (8 m^2/g, Table S1). The initial Ni/P ratio was 1/2. During TPR at high temperatures, P can form volatile P-containing compounds (PH_3 and products of its interaction with H_2O) [52,53]. However, excess P can also remain on the support surface after TPR in the form of unreduced phosphates (PO_x) ($H_nPO_4^{(3-n)-}$, $P_2O_7^{4-}$, and $(PO^{3-})_n$) [36,54,55].

To avoid blocking the SAPO-11 pores, we tested 3 wt.% NiP_I/SAPO-11 (TPR at 450 °C). To verify whether SAPO-11 is a reliable support, we tested 3 wt.% Ni/SAPO-11. Conversion values of X_{MP} = 75% and X_O = 58% were reached over Ni/SAPO-11 after 5 h of reaction (Figure 2). The NiP_I/SAPO-11 remained inactive. XRD analysis showed the presence of metallic Ni in Ni/SAPO-11 and, due to the small particle sizes, NiP_I/SAPO-11 did not have any reflexes of Ni-phosphide phases (Figure S1). This experiment showed that excess P blocks the active component in the support. As it is impossible to decrease the P content in NiP_I samples without additives (due to the poor solubility of phosphites), we used phosphate NiP_A precursors to prepare samples with different Ni/P ratios.

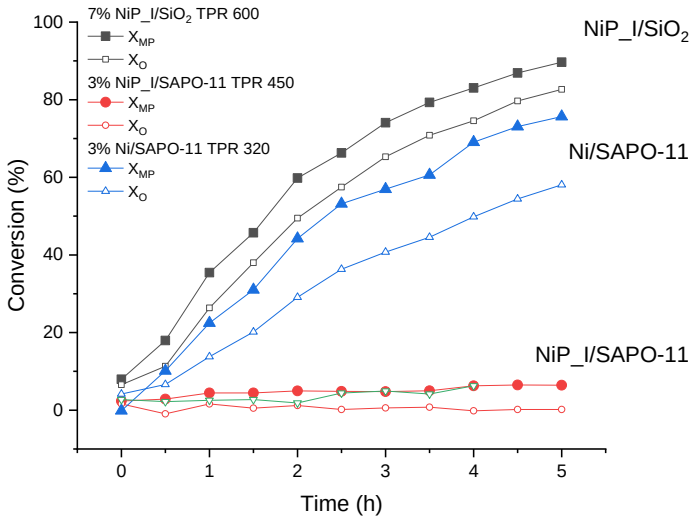

Figure 2. Conversion of MP and O-containing compounds over 7% NiP_I/SiO_2, 3% Ni/SAPO-11, and 3% NiP_I/SAPO-11 catalysts in an autoclave (290 °C, 3 MPa, V_{H2} = 100 mL/min, 500 RPM, m_{cat} = 1 g).

Depending on the Ni/P ratio, the conversion values of MP were in the range of 45–49% and the conversion values of O-containing compounds were 33–45% over the NiP_A/SAPO-11 catalyst after 5 h of reaction (Figure 3).

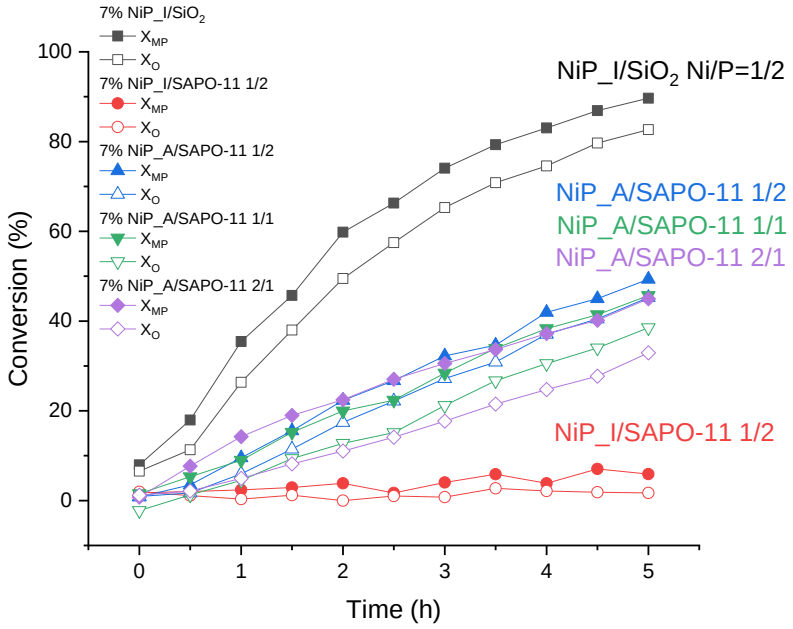

Figure 3. Conversion of MP and O-containing compounds over 7 wt.% NiP_I/SiO_2, NiP_A/SAPO-11 with different Ni/P ratios, and NiP_I/SAPO-11 in an autoclave (290 °C, 3 MPa, V_{H2} = 100 mL/min, 500 RPM, m_{cat} = 1 g).

The Ni/P ratio also influenced the selectivity (Table 1). The main products of the reaction were n-alkanes. The C_{16}/C_{15} molar ratio for NiP_A 1/2 was 0.365, for NiP_A 1/1 it was 0.168, and for NiP_A 2/1 it was 0.137. These numbers are close to the results in the literature for Ni_2P/SAPO-11 [40–42]. Figure 4 shows product distributions vs. time. MP, n-pentadecane (n-C_{15}), and n-hexadecane (n-C_{16}) concentrations vs. time are shown in Figure 4a–c, while concentrations of intermediate compounds (palmitic acid (PA), palmityl palmitate (PP), and hexadecanol (C_{16}OH)) vs. time are shown in Figure 4d–f. The selectivity to n-C_{15} and n-C_{16}

changed as follows: for Ni/P = 1/2, S_{C15} = 66% and S_{C16} = 24%; for Ni/P = 1/1, S_{C15} = 76% and S_{C16} = 13%; and for Ni/P = 2/1, S_{C15} = 60% and S_{C16} = 8% (Table 1). The overall selectivity and yield to alkanes decreased as the P content decreased, confirming the similar trend and activity dependence for SiO_2-supported Ni-phosphides [53,56]. As the P content decreased, the selectivity to O-containing intermediates and side products increased from 10% (for Ni/P = 1/2) to 31% (for Ni/P = 2/1).

Table 1. C_{16}/C_{15} molar ratios and product selectivities and yields over NiP_A catalysts with different Ni/P ratios.

Ni/P Ratio	C_{16}/C_{15} Molar Ratio	Selectivity to n-C_{15}, %	Selectivity to n-C_{16}, %	Yield of n-C_{15}, %	Yield of n-C_{16}, %
1/2	0.365	66	24	32	12
1/1	0.168	76	13	34	6
2/1	0.137	60	8	27	4

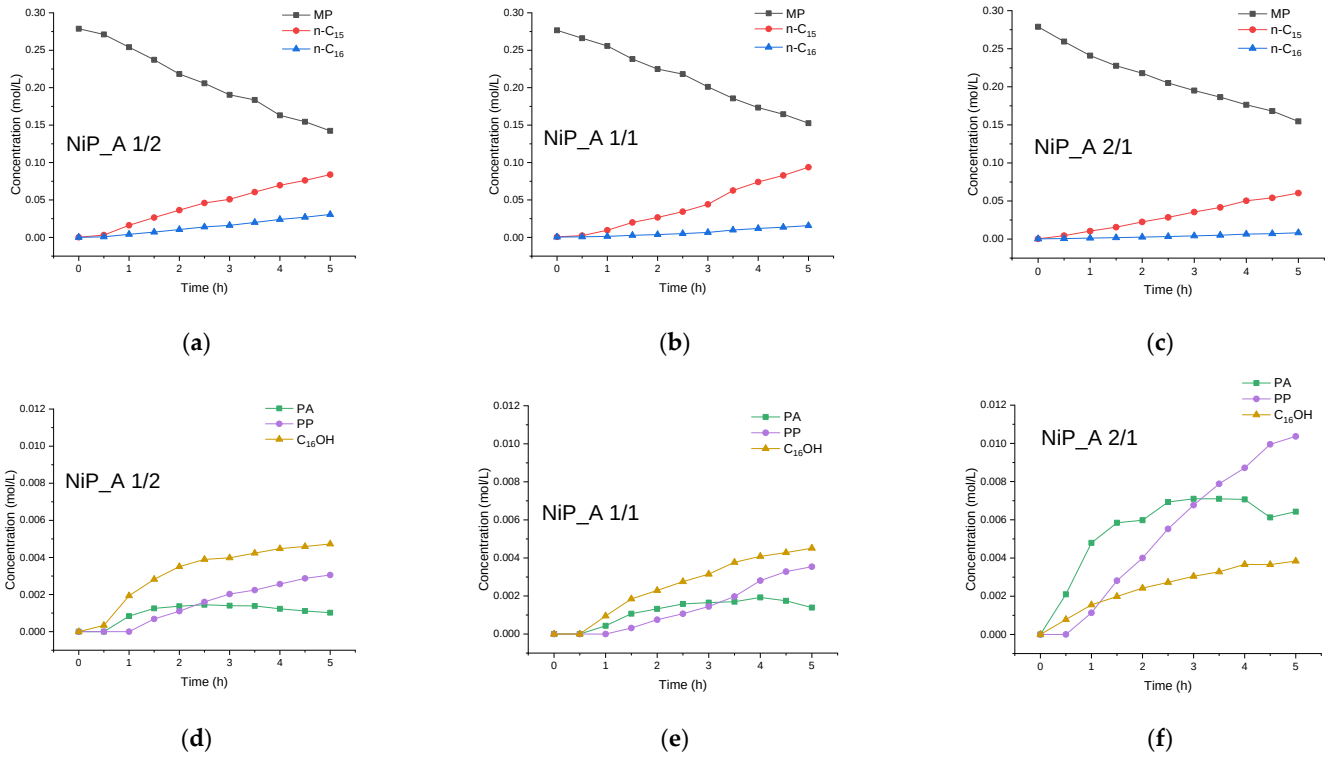

Figure 4. Concentration of reaction products vs. time in an autoclave over 7 wt.% NiP_A catalysts: (**a**,**d**) Ni/P = 1/2; (**b**,**e**) Ni/P = 1/1; (**c**,**f**) Ni/P = 2/1. MP, methyl palmitate; PA, palmitic acid; $C_{16}OH$, hexadecanol. 290 °C, 3 MPa, V_{H2} = 100 mL/min, 500 RPM, m_{cat} = 1 g.

The next step was to determine the conditions under which isomerization takes place. Screening of the NiP_A samples with different Ni contents and Ni/P ratios was conducted at 340 and 380 °C (Figure 5). At these temperatures, X_{MP} was 100%, so the selectivities are equal to the yields of the products. Catalytic experiments showed that, for the NiP_A catalyst with Ni/P = 1/2, only n-alkanes were detected both at 340 and 380 °C. Decreasing the Ni content resulted in the formation of cracked products, and no isomerized alkanes were detected (3 wt.% NiP_A, Ni/P = 1/2). Decreasing the P content in the 7 wt.% samples also contributed to the cracking; however, in the case of Ni/P = 1/1, iso-C_{15} were detected with a selectivity of 13%. For the series of 3 wt.% NiP_A catalysts with different Ni/P ratios, decreasing the P content yielded a larger number of cracked alkanes and more iso-alkanes (because of the increase in the catalyst's acidity, see Figure S2). Thus, the 3 wt.% NiP_A

catalyst with Ni/P = 2/1 has the highest selectivity to iso-alkenes (35%) (33% of iso-C_{15} and 2% of iso-C_{16}).

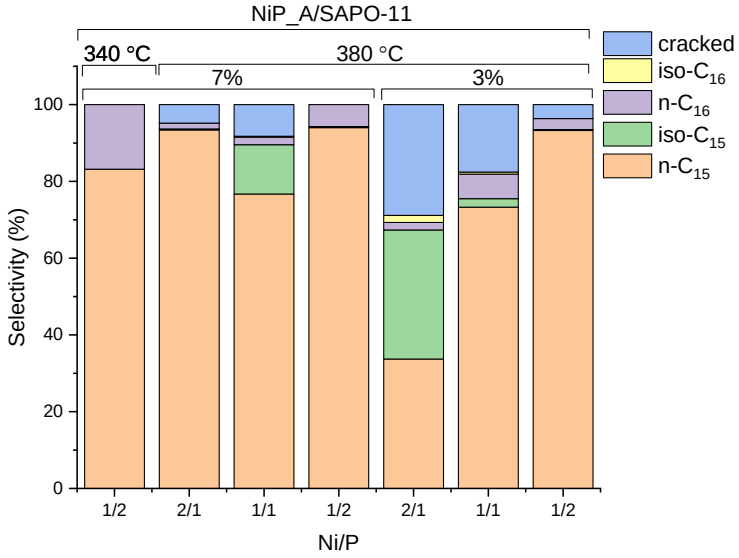

Figure 5. Product distributions after 5 h of reaction (X_{MP} = 100%) in an autoclave over NiP_A/SAPO-11 samples with different Ni contents and Ni/P molar ratios. 3 MPa, V_{H2} = 100 mL/min, 500 RPM, V_{cat} = 1.5 mL (for 7 wt.% m_{cat} = 1 g, for 3 wt.% m_{cat} = 0.85 g).

At this point, 3 wt.% NiP_A/SAPO-11 (Ni/P = 2/1) showed the highest isomerization activity, but the number of cracked products was the highest among all tested catalysts. We carried out HDO–isomerization over the 3 wt.% NiP_A series at a lower temperature (340 °C) and pressure (2 MPa) with a larger catalyst mass (1.7 g). Iso-alkanes were only obtained over the sample with Ni/P = 2/1 (35%, Figure 6). However, for this catalyst, the products were not balanced with the initial amount of MP, and no cracked products were detected. Thus, we think that 15% of the MP transformed into carbon deposits.

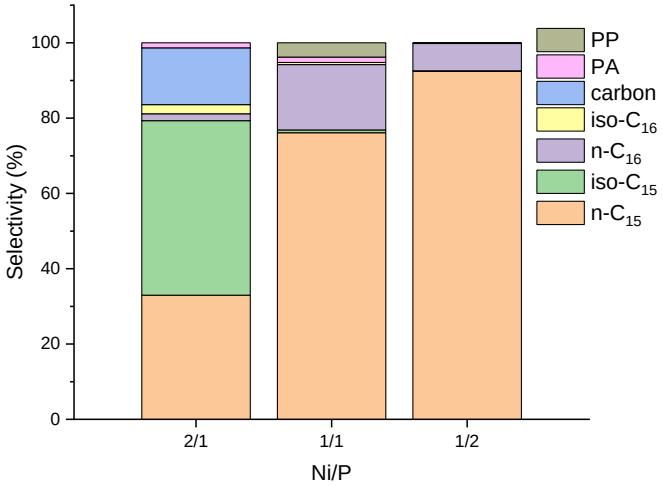

Figure 6. Product distributions after 5 h of reaction (X_{MP} = 100%) in an autoclave over 3 wt.% NiP_A/SAPO-11 samples with different Ni/P molar ratios. 340 °C, 2 MPa, V_{H2} = 100 mL/min, 500 RPM, m_{cat} = 1.7 g.

From the experimental results, we can conclude that, to obtain active catalysts simultaneously for HDO and isomerization, one needs to avoid large amounts of P in order not to block SAPO-11 pores and the active component. However, at the same time, one needs

enough P to form the Ni-phosphide and prevent cracking and cocking. The liquid phosphidation method of Ni/SAPO-11 can meet both requirements [49]. The phosphidation degree can be regulated by the temperature and duration of this procedure, and the formation of PO_x phosphate residues can be avoided [57]. This method requires a continuous-flow reactor for both phosphidation and catalytic tests.

2.1.2. Liquid-Phase Phosphidation and Experiments in a Continuous-Flow Reactor

The catalysts prepared by liquid-phase phophidation were labeled NiP_P. First, 3 wt.% Ni/SAPO-11 was phosphidized in situ by PPh_3 according to the procedure described in [49] (heating to 380 °C (1 °C/min) and holding at this temperature for 7 h (TPP380)). MP HDO–isomerization was carried out at 340 °C, 2 MPa, LHSV = 5.3 h^{-1}, and H_2/feed ratio = 600 Ncm^3/cm^3.

The NiP_P/SAPO-11 TPP380 catalyst did not show any isomerization activity (Figure 7), and 2% of the MP transformed into carbon deposits. Under the same conditions, 8% of the MP transformed into carbon deposits over the NiP_A/SAPO-11 catalyst, but the selectivity to iso-alkanes was 27% (25% of iso-C_{15}, 2% of iso-C_{16}). Thus, we decided to lower the phosphidation degree by decreasing the phosphidation temperature (250 °C, TPP250) and duration (2 h). This allowed us to obtain 40% of the iso-alkanes (33% of iso-C_{15} and 7% of iso-C_{16} over 3 wt.% NiP_P, Figure 7), but the selectivity to carbon deposits was 6%. Increasing the Ni content proved to be successful in avoiding the formation of carbon deposits and cracked products (7 wt.% NiP_P and 12 wt.% NiP_P, Figure 7) such that the mass balance was 100%. The optimal content of Ni to obtain the highest number of iso-alkanes (54% of iso-C_{15} and 12% of iso-C_{16}) was 7 wt.%. The MP conversion and selectivities of the products vs. time on stream (TOS) are shown in Figure S3.

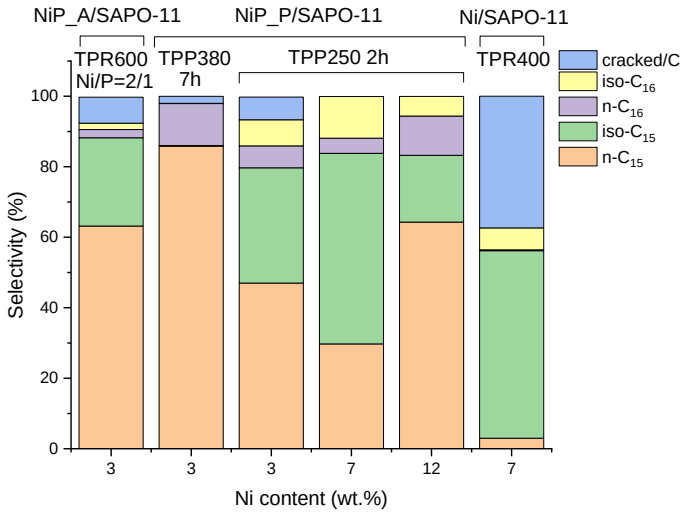

Figure 7. Product distributions over Ni-phosphide and Ni catalysts on SAPO-11 in a continuous-flow reactor (X_{MP} = 100%). T = 340 °C, 2 MPa, LHSV = 5.3 h^{-1}, 600 Ncm^3/cm^3.

Ni/SAPO-11 was also tested in continuous-flow mode in order to compare it with NiP_P/SAPO-11 (Figure 7). Despite the high selectivity to iso-alkanes (59% total), Ni/SAPO-11 had very high cracking and cocking activity (37% selectivity). Unfortunately, it was not possible to determine exactly the number of cracked products because the solvent (n-dodecane) also cracked and contributed to these products (Figure S4).

Due to the presence of metallic Ni in Ni/SAPO-11, it has high activity in methanation. There is no CO in gas phase products of Ni/SAPO-11, and high concentrations of CH_4, C_2H_6, and C_3H_8 are observed compared with Ni_2P/SAPO-11 catalysts (Figure 8). C_2H_6, C_3H_8, and additional amounts of CH_4 are produced by cracking reactions of MP, its intermediate and final products, and the n-dodecane solvent.

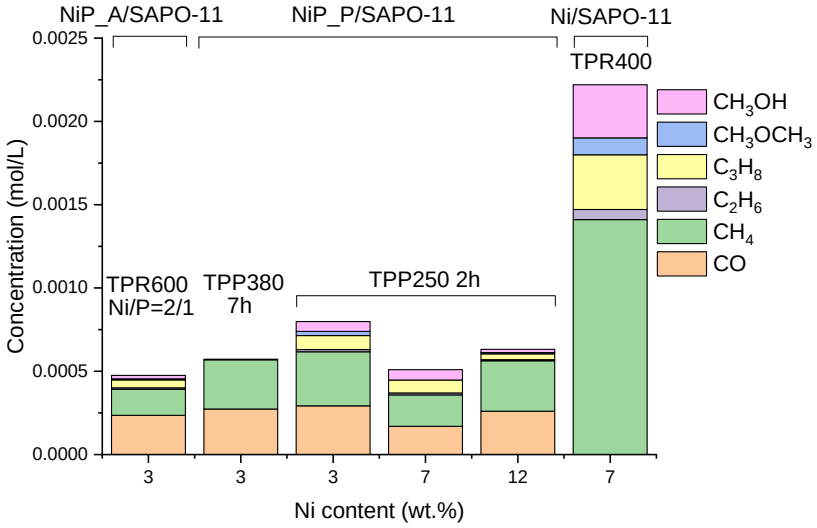

Figure 8. Distribution of gas phase products over Ni-phosphide and Ni catalysts on SAPO-11 in a continuous-flow reactor (X_{MP} = 100%). T = 340 °C, 2 MPa, LHSV = 5.3 h^{-1}, 600 Ncm^3/cm^3.

The NiP_A and NiP_P catalysts had quite similar amounts of CO and CH_4, and the most active 7 wt.% NiP_P catalyst had the lowest concentrations (Figure 8). Interestingly, there was no C_2H_6, C_3H_8, CH_3OCH_3, and CH_3OH over the NiP_P TPP380 sample.

Scheme 1 shows the possible reactions of MP HDO–isomerization. HDO has two main routes:

(1) decarbonylation: MP → PA → $C_{16}O$ → C_{15} hydrocarbons;
(2) direct HDO: MP → PA → $C_{16}O$ → $C_{16}OH$ → C_{16} hydrocarbons

where MP, methyl palmitate; PA, palmitic acid; $C_{16}O$, hexadecanal; and $C_{16}OH$, hexadecanol.

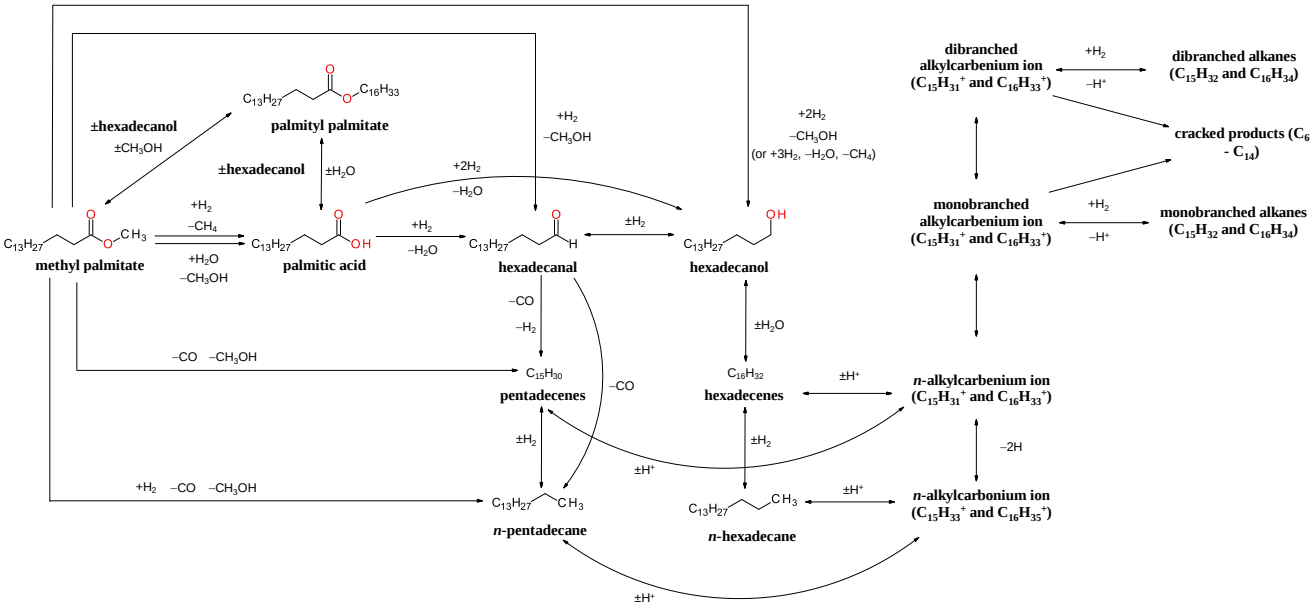

Scheme 1. Methyl palmitate HDO–isomerization.

HDO intermediates as well as palmityl palmitate are detectable at low reaction temperatures (290 °C, Figure 4). At higher temperatures (340 and 380 °C), the HDO reactions are quite fast and the conversion of O-containing compounds is complete (Figures 5– 7).

Isomerization of n-alkanes ($C_{15}H_{32}$ and $C_{16}H_{34}$) occurs through dehydration to alkenes with the subsequent formation of n-alkylcarbenium ions ($C_{15}H_{31}^+$ and $C_{16}H_{33}^+$), which form in protonation over acid sites of SAPO-11. An alternative route of n-alkylcarbenium ion formation is protonation of n-alkanes to n-alkylcarbonium ions ($C_{15}H_{33}^+$ and $C_{16}H_{35}^+$), even though this route is significantly slower [58]. The subsequent transformation of n-alkylcarbenium ions leads to monobranched alkanes, dibranched alkanes, and cracked products. According to GC-MS analysis, only trace amounts of dibranched alkanes were detected over Ni_2P/SAPO-11 catalysts. Almost all iso-alkanes are monobranched ones.

As phosphidized catalysts (TPP) are more promising and active than TPR samples, we characterized NiP_P catalysts with different Ni contents by physicochemical methods.

2.2. Physicochemical Analysis of the TPP Catalysts

2.2.1. Chemical Analysis, Textural Properties, NH_3-TPD, and XRD

The initial SAPO-11 contained 24.1 wt.% P (Table 2). Increasing the relative Ni content results in a decrease in the relative P content because P is lighter than Ni. Phosphidation increases the amount of P, but its effect was negligible compared with the overall P content in SAPO-11 and changed due to the Ni loading.

Table 2. Physicochemical properties of NiP_P samples.

	Ni, wt.%	P, wt.%	V_{micro}, cm^3/g	V_{meso}, cm^3/g	S_{micro}, m^2/g	S_{BET}, m^2/g	NH_3-TPD, μmol/g	XRD Phase	D_{XRD}, nm	D_{TEM}, nm
SAPO-11	–	24.1	0.064	0.08	166	188	161	–	–	–
3% NiP_P	3.4	21.3	0	0.12	0	19.5	122	Ni_2P	30	6.5
7% NiP_P	7.3	20.9	0	0.10	0	16.0	110	Ni_2P	59	9.2
12% NiP_P	12.0	20.3	0	0.10	0	17.6	145	Ni_2P	39	9.9

The S_{BET} of the NiP_P samples was significantly lower than the S_{BET} of the original SAPO-11 (Table 2). This may have been due to blocking of the SAPO-11 pores by the active component and excess P. It resulted in the absence of micropores, as $V_{micro} = 0$ cm^3/g and $S_{micro} = 0$ m^2/g. The pore size distributions of the support and the catalysts are shown in Figure S5.

The acidity of the catalysts was lower than for SAPO-11 (Table 2, Figure 9). In the NH_3-TPD curve of SAPO-11, there are two main signals with maximums at ~180 °C and ~300 °C. The first signal corresponds to weak acid sites, and the second signal corresponds to medium-strength acid sites [26,43]. These signals remain in the NiP_P samples, but an additional broad signal appears after phosphidation at ~500 °C. This may correspond to the formation of volatile P-containing compounds at high temperatures of NH_3-TPD. The acidity of the 12% sample is the highest among the NiP_P catalysts (145 μmol/g), and the acidity of the 3 and 7% samples is similar (122 and 110 μmol/g, respectively).

Figure 10 shows XRD patterns of NiP_P samples with different Ni contents. All catalysts contain the Ni_2P phase. Table 1 lists the D_{XRD} of Ni_2P particles, and it is quite large (30–59 nm). It should be noted that small particles (<3 nm) could not be detected by XRD; therefore, the D_{XRD} is larger than the D_{TEM}.

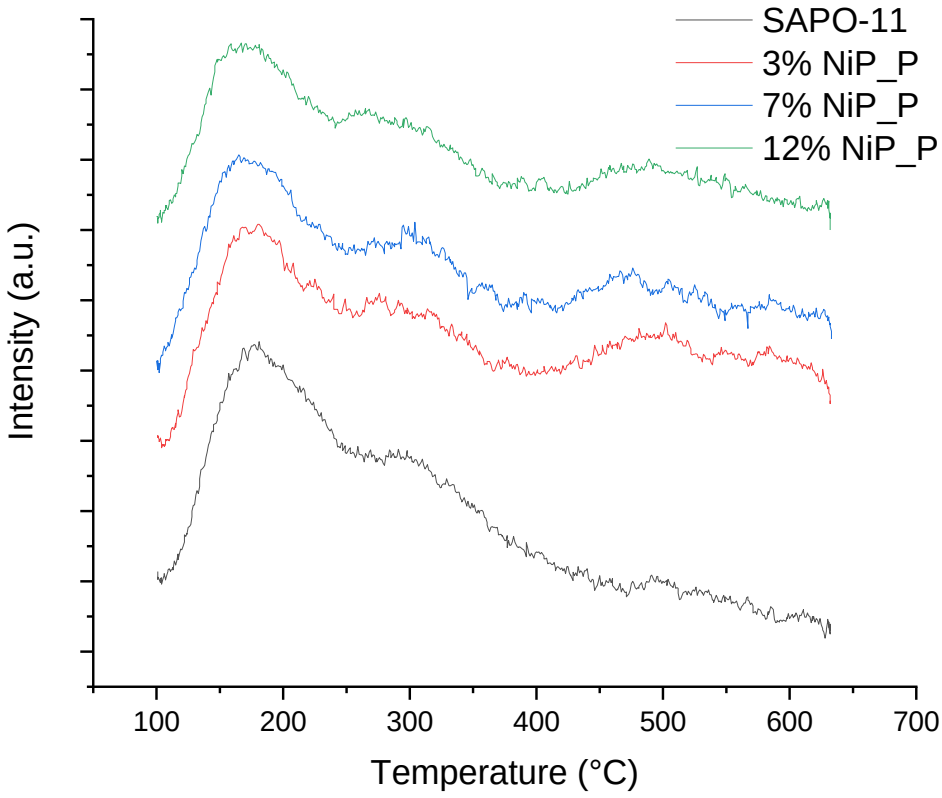

Figure 9. NH_3-TPD of SAPO-11 and the NiP_P samples.

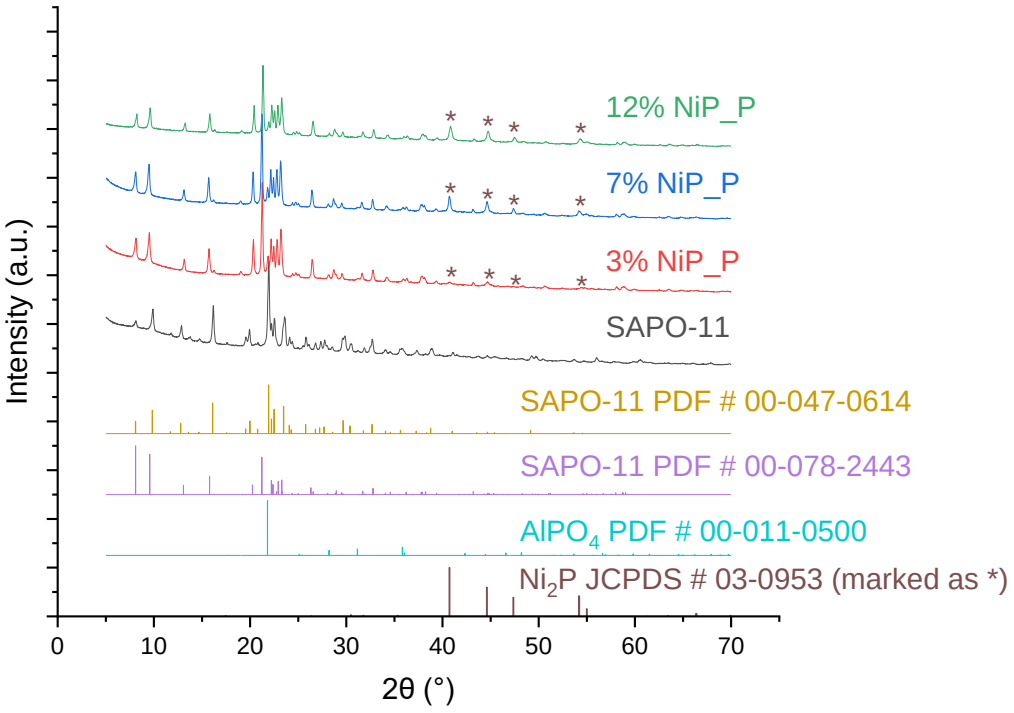

Figure 10. XRD patterns of the NiP_P samples and the SAPO-11 support.

2.2.2. TEM and SEM Analysis

The initial SAPO-11 support consisted of agglomerates of elongated particles with sizes of ~1 µm (Figure S6). TEM images of the NiP_P catalysts show that the SAPO-11 particles are evenly covered with Ni_2P nanoparticles (Figure 11).

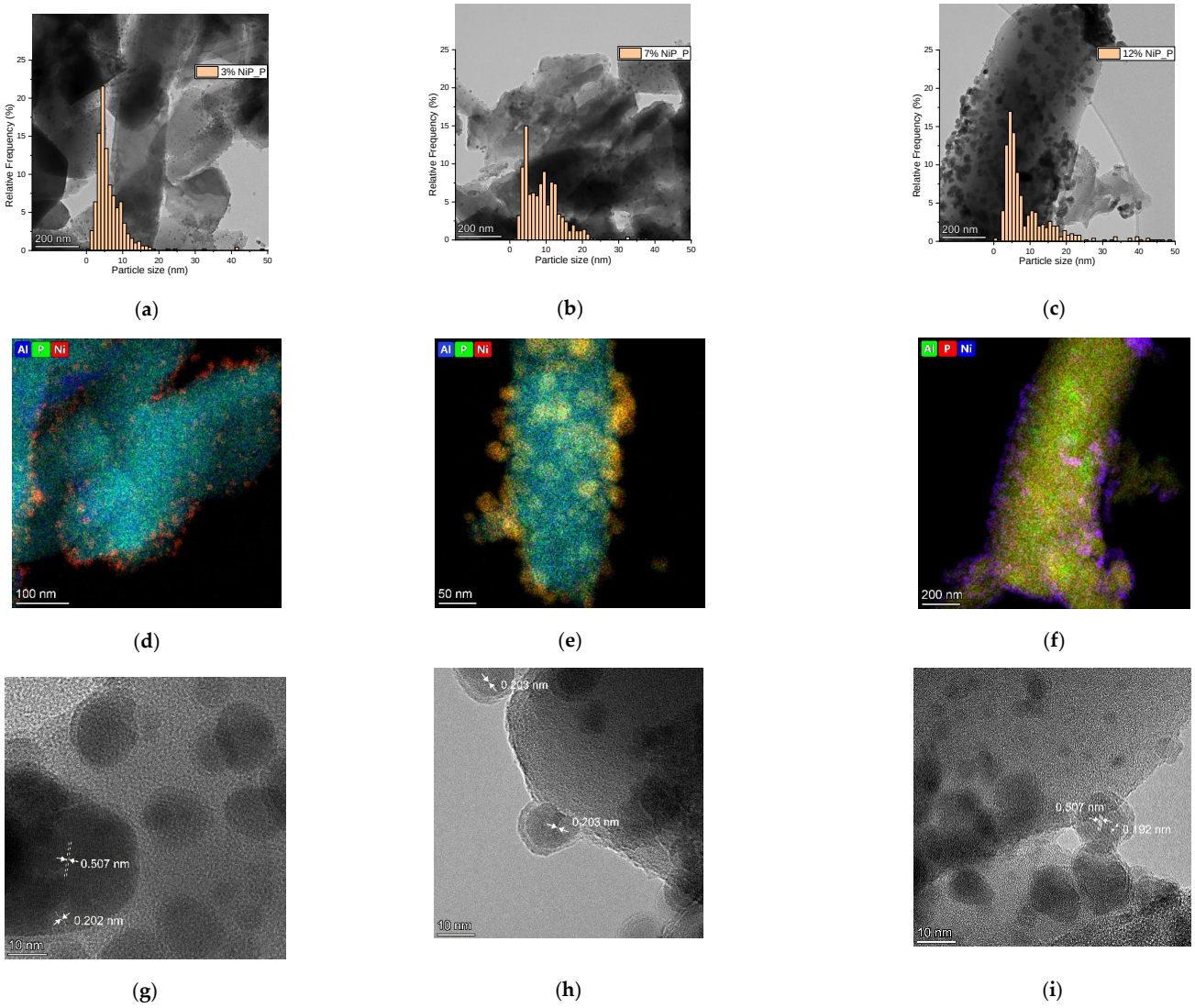

Figure 11. TEM images of: (**a**,**d**,**g**) 3% NiP_P; (**b**,**e**,**h**) 7% NiP_P; (**c**,**f**,**i**) 12% NiP_P.

Figure 11a–c show TEM images and particle size distributions of NiP_P samples with different Ni contents. All the distributions have a maximum at 4.5 nm. As the Ni content increased, the distributions became broader and bimodal for 7% NiP_P and 12% NiP_P. The mean values (D_{TEM}) of particle sizes are listed in Table 1. The D_{TEM} increased from 6.5 nm to 9.9 nm as the Ni content increased. EDX mapping showed the presence of Ni-phosphide particles on SAPO-11 (Figure 11d–f). All particles were covered with an oxidized layer, which mainly consisted of $Ni_3(PO)_4$ according to the EDX analysis (Figure 11g–i). Interplanar distances were identified for several particles (Figure 11g–i): 0.192, 0.202, 0.203, and 0.507 nm. These distances correspond to the Ni_2P crystal structure (Ni_2P JCPDS # 03-0953). The distances are related to the (210), (201), and (100) XRD reflexes, respectively.

3. Materials and Methods

3.1. Materials

For SAPO-11 synthesis, H_3PO_4 (85 wt.%, analytical grade) from «Spektrchem» (Saint Petersburg, Russia), SiO_2 Rosil-175 powder (90%, grade B) from JSC «BSK» (Sterlitamak, Russia), and hydrated alumina/oxide–hydroxide alumina were used (JSC «Promcatalys», Ryazan, Russia). Dipropylamine (DPA, 99%) from «Acros Organics» (Newark, NJ, USA) was used as a molecular template. SiO_2 was purchased from «KhromAnalit» LTd. (KSKG-type, Moscow, Russia). $Ni(CH_3CH_2COO)_2{\cdot}4H_2O$ was purchased from «Reachim» (GOST

11125-84, ≥98%, Moscow, Russia). $(NH_4)_2HPO_4$ was purchased from «Alfa Aesar» (Technical Grade, Kandel, Germany). $Ni(OH)_2$ was purchased from «Acros Organics» (≥98%, NJ, USA). H_3PO_3 was purchased from «Sigma-Aldrich» (≥97%, Burlington, MA, USA).

Methyl palmitate ($C_{15}H_{31}COOCH_3$) was purchased from «Sigma-Aldrich» (≥97%, Burlington, USA), n-dodecane was purchased from «Acros Organics» (≥98%, NJ, USA), and PPh_3 was purchased from «Sigma-Aldrich» (99%, Burlington, USA).

3.2. SAPO-11 Synthesis

SAPO-11 was synthesized via conventional hydrothermal synthesis (HTS) in an autoclave with a volume of 10 L. Aluminum and phosphorus precursors were mixed together with the subsequent addition of DPA and a silica source. All precursors were mixed until the reaction mixture became homogeneous. The final reaction mixture underwent hydrothermal synthesis at 200 °C for 24 h under stirring during HTS.

The initial molar composition contained $Al_2O_3/P_2O_5/SiO_2 = 1/1/0.1$. The amount of molecular template used was in the range of 0.9–1.5 moles to 1 mol of Al_2O_3.

After synthesis, the product was collected, washed with distilled water from the mother liquor, dried, and calcined at 650 °C with a heating rate of 3 °C/min to remove the organic template.

3.3. NiP/SAPO-11 and NiP/SiO_2 Synthesis

SAPO-11 powders or SiO_2 granules (0.25–0.5 mm) were incipiently impregnated with aqueous solutions of precursors.

NiP_A (phosphate samples). To prepare phosphate precursors, $(NH_4)_2HPO_4$ was dissolved in distilled water. Then, $Ni(CH_3CH_2COO)_2{\cdot}4H_2O$ was added. A green-yellow precipitate of Ni-phosphate was formed, which was then dissolved by the dropwise addition of concentrated HNO_3. The supports were impregnated by this solution. The samples were dried overnight at room temperature, then at 110 °C for 3 h. Afterwards, the samples were calcined at 500 °C for 3 h. To form phosphides, the precursors were reduced in a hydrogen flow (250 mL/min) using the following temperature program: heating to 380 °C on a 3 °C/min ramp, then heating to 600 °C on a 1 °C/min ramp. The content of Ni in the reduced catalysts was ~3 or ~7 wt.%. The content of P was varied using different initial Ni/P molar ratios (2/1, 1/1, and 1/2) in the precursors.

NiP_I (phosphite samples). To prepare phosphite samples, the precursor $Ni(OH)_2$ was dissolved in a H_3PO_3 water solution. The initial Ni/P molar ratio was 1/2. The supports were impregnated by this solution. The samples were dried overnight at room temperature, then at 80 °C for 24 h. Then, the precursors were reduced in a hydrogen flow (250 mL/min) using the following temperature program: heating to 600 °C on a 1 °C/min ramp. The content of Ni in the reduced catalysts was ~3 or ~7 wt.%.

NiP_P (liquid phosphidation samples). To prepare metallic samples for liquid phosphidation, $Ni(CH_3CH_2COO)_2{\cdot}4H_2O$ was dissolved in distilled water. The green solution was used to impregnate the supports. The samples were dried overnight at room temperature, then at 110 °C for 3 h. Then, the precursors were calcined at 400 °C for 3 h. The content of Ni after calcination was ~3, ~7, or ~12 wt.%. The oxide precursors were reduced in situ in a continuous-flow fixed-bed reactor at 400 °C for 2 h (on a 1 °C/min ramp). After cooling, phosphidation was carried out using 2 wt.% PPh_3 in dodecane (LHSV = 5.3 h^{-1}, P_{H2} = 0.5 MPa, H_2/feed = 600 Ncm^3/cm^3) with heating to 250 °C at 1 °C/min and holding at 250 °C for 2 h.

3.4. Catalyst Characterization

Elemental analysis was performed by inductively coupled plasma atomic emission spectroscopy (ICP-AES) on an Optima 4300 DV («Perkin Elmer», Waltham, MA, USA).

Textural properties were determined by N_2 physisorption on an ASAP 2400 («Micromeritics», Norcross, GA, USA).

NH_3-TPD analysis was carried out using a Chemosorb («Neosib» LTd., Novosibirsk, Russia). A total of 200 mg of sample was preheated for 1 h in He flow (60 mL/min) at 500 °C. The adsorption of NH_3 was carried out at 100 °C for 1 h. Then, to remove physically adsorbed ammonia, the sample was kept at 100 °C for 1 h in He flow (60 mL/min). Desorption was carried out at a heating rate of 10 °C/min in He flow (60 mL/min). Desorbed NH_3 was determined by a thermal conductivity detector.

X-ray diffraction analysis (XRD) was performed on an XTRA diffractometer («Thermo Fisher Scientific», Waltham, MA, USA) using CuKα radiation (wavelength λ = 1.5418 Å).

TEM microphotographs were obtained on a JEM-2010 («JEOL», Tokyo, Japan) transmission electron microscope with an accelerating voltage of 200 kV and a resolution of 0.14 nm.

3.5. Catalytic Experiments

Screening of the HDO–isomerization activity of the NiP_A and NiP_I catalysts was carried out in a 300 mL «Autoclave Engineers» (Erie, PA, USA) Bolted Pressure Vessel Closure (Autoclave reactor) in semi-batch mode (H_2 continuous flow). For a typical experiment, the catalyst was reduced ex situ, then transferred under Ar to the reactor and heated to 180 °C in H_2 flow (100 mL/min). Subsequently, 100 mL of 10% MP in n-dodecane was added to the reactor, the pressure was set to 3 MPa, and the temperature was set to 290–380 °C. When the temperature reached the reaction temperature, mixing was started (500 RPM).

NiP_P catalysts were prepared and tested in a continuous-flow fixed-bed reactor (i.d. = 12 mm) with a coaxial thermocouple with a diameter of 3 mm. The precursors were reduced and phosphidized; then, after the catalyst was cooled and washed with n-dodecane, HDO–isomerization of MP (10 wt.% in n-dodecane) was carried out at 250–340 °C, 2 MPa, LHSV = 5.3 h^{-1}, and H_2/feed = 600 Ncm^3/cm^3.

Liquid products were analyzed by a gas chromatograph («Agilent» N6890, Santa Clara, CA, USA) with an HP-1 MS column (30 m × 0.32 mm × 1 μm) and a flame ionization detector (FID). O content was determined by a Vario EL Cube elemental analyzer (Elementar Analysensysteme GmbH, Langenselbold, Germany). Gas-phase products were analyzed by a gas chromatograph («Chromos 1000», Dzerzhinsk, Russia) with a packed column (with HayeSep, «Sigma-Aldrich», Burlington, USA), methanator with a Pd catalyst, and an FID.

The conversion of MP was calculated as follows:

$$X_{MP} = \left(\frac{C^0_{MP} - C_{MP}}{C^0_{MP}} \right) \cdot 100\%, \quad (1)$$

where C^0_{MP} is the initial concentration of MP and C_{MP} is the MP concentration in the products.

The conversion of O-containing compounds was calculated as follows:

$$X_O = \left(\frac{C^0_O - C_O}{C^0_O} \right) \cdot 100\%, \quad (2)$$

where C^0_O is the initial concentration of oxygen and C_O is the concentration of oxygen in the products.

The selectivity was calculated as follows:

$$S_i = \left(\frac{C_i}{C^0_{MP} - C_{MP}} \right) \cdot 100\%, \quad (3)$$

where C_i is the concentration of the i-th compound in the products. For cracked products and carbon deposits, selectivity was estimated based on mass balance.

The yield was calculated as follows:

$$Y_i = \left(\frac{C_i}{C^0_{MP}} \right) \cdot 100\%. \quad (4)$$

4. Conclusions

The activity in HDO–isomerization of MP over SAPO-11-supported Ni-phosphide catalysts proved to depend on the preparation method and the phosphidation degree of the catalysts. NiP_I/SAPO-11 (the phosphite precursor) did not show activity in both HDO and isomerization. This was attributed to unreduced PO_x residues that blocked the surface of the catalyst and the active component. NiP_A/SAPO-11 (the phosphate precursor) activity correlated with the Ni content and Ni/P molar ratio. A low Ni loading (3 wt.%) and low P content (Ni/P = 2/1) resulted in the formation of iso-C_{15} and iso-C_{16} hydrocarbons. The selectivity to iso-alkanes at 340 °C, 2 MPa, and at full conversion in a semi-batch autoclave was 35%. At the same time, the selectivity to carbon deposits was 15%. In the continuous-flow reactor, the same catalyst produced 27% of the iso-alkanes and 8% of the carbon deposits (at T = 340 °C, 2 MPa, LHSV = 5.3 h^{-1}, and H_2/feed = 600 Ncm^3/cm^3). This catalyst has a metallic character that is too strong, which results in a high degree of cracking activity. In situ liquid-phase phosphidation by PPh_3 allowed us to finely tune the phosphidation degree of the Ni_2P/SAPO-11 catalysts (NiP_P) in order to make them suitable for simultaneous HDO–isomerization. The highest selectivity to iso-alkanes was 66% (54% of iso-C_{15} and 12% of iso-C_{16}) for 7 wt.% NiP_P/SAPO-11 phosphidized at 250 °C for 2 h. No carbon deposits formed over this catalyst.

The evidence from this study suggests that liquid-phase phosphidation is an effective way to prepare Ni_2P/SAPO-11 catalysts for one-pot HDO–isomerization of fatty esters.

Supplementary Materials: The following supporting information can be downloaded at: https://www.mdpi.com/article/10.3390/catal12111486/s1, Table S1: Textural properties of SAPO-11 and NiP_I/SAPO-11 samples; Figure S1: XRD patterns of Ni/SAPO-11 and NiP_I/SAPO-11 samples; Figure S2: NH_3-TPD curves of 3% NiP_A samples; Figure S3: X_{MP} and selectivities of the products vs. time on stream (TOS) over (a) 3% NiP_A/SAPO-11 TPR 600 Ni/P = 2/1, (b) 3% NiP_P/SAPO-11 TPP380 7h, (c) 3% NiP_P/SAPO-11 TPP250 2h, (d) 7% NiP_P/SAPO-11 TPP250 2h, (e) 12% NiP_P/SAPO-11 TPP250 2h, and (f) 3% Ni/SAPO-11 TPR400 in a continuous-flow reactor. T = 340 °C (2 MPa, LHSV = 5.3 h^{-1}, 600 Ncm^3/cm^3); Figure S4: Chromatograms of the products after 8 h of TOS over Ni-phosphide and Ni catalysts on SAPO-11 in a continuous-flow reactor (X_{MP} = 100%) (T = 340 °C, 2 MPa, LHSV = 5.3 h^{-1}, 600 Ncm^3/cm^3); Figure S5: Pore size distributions of SAPO-11 and NiP_P samples; Figure S6: SEM image of the SAPO-11 support.

Author Contributions: Conceptualization, I.V.S.; formal analysis, I.V.S. and I.A.S.; investigation, I.V.S. and I.A.S.; writing—original draft preparation, I.V.S.; writing—review and editing, I.V.S. and I.A.S.; SAPO-11 preparation, I.A.S.; supervision, E.V.P. and G.A.B. All authors have read and agreed to the published version of the manuscript.

Funding: This work was supported by the Russian Science Foundation (grant no. 22-13-00371). The work concerning the preparation of SAPO-11 was supported by the Ministry of Science and Higher Education of the Russian Federation within the governmental order for the Boreskov Institute of Catalysis (project AAAA-A21-121011490008–3).

Data Availability Statement: Not applicable.

Acknowledgments: The authors of the paper are grateful to M.V. Shashkov for the analysis and identification of HDO–isomerization products by GC/MS, A.B. Ayupov for the N_2 adsorption analysis, V.P. Pakharukova for the XRD analysis, and E.Y. Gerasimov for the TEM analysis.

Conflicts of Interest: The authors declare no conflict of interest.

References

1. Di Vito Nolfi, G.; Gallucci, K.; Rossi, L. Green Diesel Production by Catalytic Hydrodeoxygenation of Vegetables Oils. *Int. J. Environ. Res. Public Health* **2021**, *18*, 13041. [CrossRef] [PubMed]
2. Yeletsky, P.M.; Kukushkin, R.G.; Yakovlev, V.A.; Chen, B.H. Recent Advances in One-Stage Conversion of Lipid-Based Biomass-Derived Oils into Fuel Components—Aromatics and Isomerized Alkanes. *Fuel* **2020**, *278*, 118255. [CrossRef]
3. Monteiro, R.R.C.; dos Santos, I.A.; Arcanjo, M.R.A.; Cavalcante, C.L.; de Luna, F.M.T.; Fernandez-Lafuente, R.; Vieira, R.S. Production of Jet Biofuels by Catalytic Hydroprocessing of Esters and Fatty Acids: A Review. *Catalysts* **2022**, *12*, 237. [CrossRef]
4. Aslam, M.; Kumar, H.; Sarma, A.K.; Kumar, P. Current Status of the Green Diesel Industry. In *Green Diesel: An Alternative to Biodiesel and Petrodiesel*; Aslam, M., Shivaji Maktedar, S., Sarma, A.K., Eds.; Advances in Sustainability Science and Technology; Springer Nature: Singapore, 2022; pp. 265–283. ISBN 978-981-19223-5-0.
5. Li, X.; Luo, X.; Jin, Y.; Li, J.; Zhang, H.; Zhang, A.; Xie, J. Heterogeneous Sulfur-Free Hydrodeoxygenation Catalysts for Selectively Upgrading the Renewable Bio-Oils to Second Generation Biofuels. *Renew. Sustain. Energy Rev.* **2018**, *82*, 3762–3797. [CrossRef]
6. Long, F.; Liu, W.; Jiang, X.; Zhai, Q.; Cao, X.; Jiang, J.; Xu, J. State-of-the-Art Technologies for Biofuel Production from Triglycerides: A Review. *Renew. Sustain. Energy Rev.* **2021**, *148*, 111269. [CrossRef]
7. Mäki-Arvela, P.; Martínez-Klimov, M.; Murzin, D.Y. Hydroconversion of Fatty Acids and Vegetable Oils for Production of Jet Fuels. *Fuel* **2021**, *306*, 121673. [CrossRef]
8. Shamanaeva, I.A.; Yu, Z.; Utemov, A.V.; Wu, W.; Sladkovskiy, D.A.; Parkhomchuk, E.V. Role of Texture and Acidity of SAPO-34 in Methanol to Olefins Conversion. *Pet. Chem.* **2020**, *60*, 471–478. [CrossRef]
9. Wang, L.; Meng, F.; Li, B.; Zhang, J.; Li, Z. A Dual-Bed Strategy for Direct Conversion of Syngas to Light Paraffins. *Catalysts* **2022**, *12*, 967. [CrossRef]
10. Xiao, X.; Xu, Z.; Wang, P.; Liu, X.; Fan, X.; Kong, L.; Xie, Z.; Zhao, Z. Solvent-Free Synthesis of SAPO-34 Zeolite with Tunable SiO2/Al2O3 Ratios for Efficient Catalytic Cracking of 1-Butene. *Catalysts* **2021**, *11*, 835. [CrossRef]
11. Porsin, A.A.; Vlasova, E.N.; Nuzhdin, A.L.; Aleksandrov, P.V.; Bukhtiyarova, G.A. Co-Processing of Straight Run Gas Oil-Rapeseed Oil Mixture Using Sulfide NiMo Catalyst on Zeolite-Containing Support. *Russ. J. Appl. Chem.* **2019**, *92*, 1797–1804. [CrossRef]
12. Pimerzin, A.; Savinov, A.; Vutolkina, A.; Makova, A.; Glotov, A.; Vinokurov, V.; Pimerzin, A. Transition Metal Sulfides- and Noble Metal-Based Catalysts for N-Hexadecane Hydroisomerization: A Study of Poisons Tolerance. *Catalysts* **2020**, *10*, 594. [CrossRef]
13. Vlasova, E.N.; Porsin, A.A.; Aleksandrov, P.V.; Nuzhdin, A.L.; Bukhtiyarova, G.A. Co-Hydroprocessing of Straight-Run Gasoil—Rapeseed Oil Mixture over Stacked Bed Mo/Al2O3 + NiMo/Al2O3-SAPO-11 Catalysts. *Fuel* **2021**, *285*, 119504. [CrossRef]
14. Vlasova, E.N.; Porsin, A.A.; Aleksandrov, P.V.; Nuzhdin, A.L.; Bukhtiyarova, G.A. Co-processing of Rapeseed Oil—Straight Run Gas Oil Mixture: Comparative Study of Sulfide CoMo/Al2O3-SAPO-11 and NiMo/Al2O3-SAPO-11 Catalysts. *Catal. Today* **2021**, *378*, 119–125. [CrossRef]
15. Grenev, I.V.; Klimkin, N.D.; Shamanaeva, I.A.; Shubin, A.A.; Chetyrin, I.A.; Gavrilov, V.Y. A Novel Adsorption-Based Method for Revealing the Si Distribution in SAPO Molecular Sieves: The Case of SAPO-11. *Microporous Mesoporous Mater.* **2021**, *328*, 111503. [CrossRef]
16. Freitas, C.; Pereira, M.; Souza, D.; Fonseca, N.; Sales, E.; Frety, R.; Felix, C.; Azevedo, A.; Brandao, S. Thermal and Catalytic Pyrolysis of Dodecanoic Acid on SAPO-5 and Al-MCM-41 Catalysts. *Catalysts* **2019**, *9*, 418. [CrossRef]
17. Auwal, I.A.; Wong, K.-L.; Ling, T.C.; Ooi, B.S.; Ng, E.-P. Metal Chlorides Grafted on SAPO-5 (MClx/SAPO-5) as Reusable and Superior Catalysts for Acylation of 2-Methylfuran Under Non-Microwave Instant Heating Condition. *Processes* **2020**, *8*, 603. [CrossRef]
18. Yang, Y.; Liu, X.; Lyu, Y.; Liu, Y.; Zhan, W.; Yu, Z.; Fan, L.; Yan, Z. Enhanced Dispersion of Nickel Nanoparticles on SAPO-5 for Boosting Hydroisomerization of n-Hexane. *J. Colloid Interface Sci.* **2021**, *604*, 727–736. [CrossRef]
19. Yang, J.; Kikhtyanin, O.V.; Wu, W.; Zhou, Y.; Toktarev, A.V.; Echevsky, G.V.; Zhang, R. Influence of the Template on the Properties of SAPO-31 and Performance of Pd-Loaded Catalysts for n-Paraffin Isomerization. *Microporous Mesoporous Mater.* **2012**, *150*, 14–24. [CrossRef]
20. Smirnova, M.Y.; Kikhtyanin, O.V.; Smirnov, M.Y.; Kalinkin, A.V.; Titkov, A.I.; Ayupov, A.B.; Ermakov, D.Y. Effect of Calcination Temperature on the Properties of Pt/SAPO-31 Catalyst in One-Stage Transformation of Sunflower Oil to Green Diesel. *Appl. Catal. A Gen.* **2015**, *505*, 524–531. [CrossRef]
21. Echevskii, G.V.; Weixin, Q.; Kodenev, E.G.; Toktarev, A.V.; Chunmei, D. Study of Bifunctional Hydrocracking and Hydroisodeparaffinization Catalysts Based on Zeolites and Alumophosphates, Part 2: Effect of the Activity of Hydrogenating and Acidic Components on the Activity and Selectivity of Hydroisodeparaffinization Catalysts. *Catal. Ind.* **2020**, *12*, 81–87. [CrossRef]
22. Wei, X.; Kikhtyanin, O.V.; Parmon, V.N.; Wu, W.; Bai, X.; Zhang, J.; Xiao, L.; Su, X.; Zhang, Y. Synergetic Effect between the Metal and Acid Sites of Pd/SAPO-41 Bifunctional Catalysts in n-Hexadecane Hydroisomerization. *J. Porous Mater.* **2018**, *25*, 235–247. [CrossRef]
23. Phan, D.-P.; Lee, E.Y. Catalytic Hydroisomerization Upgrading of Vegetable Oil-Based Insulating Oil. *Catalysts* **2018**, *8*, 131. [CrossRef]
24. Jia, G.; Guo, C.; Wang, W.; Bai, X.; Wei, X.; Su, X.; Li, T.; Xiao, L.; Wu, W. The Synergic Effects of Highly Selective Bimetallic Pt-Pd/SAPO-41 Catalysts for the n-Hexadecane Hydroisomerization. *Front. Chem. Sci. Eng.* **2021**, *15*, 1111–1124. [CrossRef]

25. Tiuliukova, I.A.; Rudina, N.A.; Lysikov, A.I.; Cherepanova, S.V.; Parkhomchuk, E.V. Screw-like Morphology of Silicoaluminophosphate-11 (SAPO-11) Crystallized in Ethanol Medium. *Mater. Lett.* **2018**, *228*, 61–64. [CrossRef]
26. Shamanaeva, I.A.; Parkhomchuk, E.V. Variability of Molecular Sieve SAPO-11 Crystals: Acidity, Texture, and Morphology. *J. Porous Mater.* **2022**, *29*, 481–492. [CrossRef]
27. Yadav, R.; Singh, A.K. Recent Developments on Clean Fuels over SAPO-Type Catalysts. In *Catalysis for Clean Energy and Environmental Sustainability: Petrochemicals and Refining Processes—Volume 2*; Pant, K.K., Gupta, S.K., Ahmad, E., Eds.; Springer International Publishing: Cham, Switzerland, 2021; pp. 503–525. ISBN 978-3-030-65021-6.
28. Shamanaeva (Tiuliukova), I.A.; Parkhomchuk, E.V. Influence of the Precursor Preparation Procedure on the Physicochemical Properties of Silicoaluminophosphate SAPO-11. *Pet. Chem.* **2019**, *59*, 854–859. [CrossRef]
29. Ahmad, S.; Ashraf, I.; Mansoor, M.A.; Rizwan, S.; Iqbal, M. An Overview of Recent Advances in the Synthesis and Applications of the Transition Metal Carbide Nanomaterials. *Nanomaterials* **2021**, *11*, 776. [CrossRef]
30. Smith, K.J. Metal Carbides, Phosphides, and Nitrides for Biomass Conversion. *Curr. Opin. Green Sustain. Chem.* **2020**, *22*, 47–53. [CrossRef]
31. Hasanudin, H.; Ryan Asri, W.; Said, M.; Tamara Hidayati, P.; Purwaningrum, W.; Novia, N.; Wijaya, K. Hydrocracking Optimization of Palm Oil to Bio-Gasoline and Bio-Aviation Fuels Using Molybdenum Nitride-Bentonite Catalyst. *RSC Adv.* **2022**, *12*, 16431–16443. [CrossRef]
32. Hasanudin, H.; Ryan Asri, W.; Sari Zulaikha, I.; Ayu, C.; Rachmat, A.; Riyanti, F.; Hadiah, F.; Zainul, R.; Maryana, R. Hydrocracking of Crude Palm Oil to a Biofuel Using Zirconium Nitride and Zirconium Phosphide-Modified Bentonite. *RSC Adv.* **2022**, *12*, 21916–21925. [CrossRef]
33. Alvarez-Galvan, M.C.; Campos-Martin, J.M.; Fierro, J.L.G. Transition Metal Phosphides for the Catalytic Hydrodeoxygenation of Waste Oils into Green Diesel. *Catalysts* **2019**, *9*, 293. [CrossRef]
34. Golubeva, M.A.; Zakharyan, E.M.; Maximov, A.L. Transition Metal Phosphides (Ni, Co, Mo, W) for Hydrodeoxygenation of Biorefinery Products (a Review). *Pet. Chem.* **2020**, *60*, 1109–1128. [CrossRef]
35. Al-Ali, L.I.; Elmutasim, O.; Al Ali, K.; Singh, N.; Polychronopoulou, K. Transition Metal Phosphides (TMP) as a Versatile Class of Catalysts for the Hydrodeoxygenation Reaction (HDO) of Oil-Derived Compounds. *Nanomaterials* **2022**, *12*, 1435. [CrossRef]
36. Shamanaev, I.; Deliy, I.; Aleksandrov, P.; Gerasimov, E.; Pakharukova, V.; Kodenev, E.; Ayupov, A.; Andreev, A.; Lapina, O.; Bukhtiyarova, G. Effect of Precursor on the Catalytic Properties of Ni_2P/SiO_2 in Methyl Palmitate Hydrodeoxygenation. *RSC Adv.* **2016**, *6*, 30372–30383. [CrossRef]
37. Deliy, I.V.; Shamanaev, I.V.; Aleksandrov, P.V.; Gerasimov, E.Y.; Pakharukova, V.P.; Kodenev, E.G.; Yakovlev, I.V.; Lapina, O.B.; Bukhtiyarova, G.A. Support Effect on the Performance of Ni2P Catalysts in the Hydrodeoxygenation of Methyl Palmitate. *Catalysts* **2018**, *8*, 515. [CrossRef]
38. Shamanaev, I.V.; Deliy, I.V.; Aleksandrov, P.V.; Reshetnikov, S.I.; Bukhtiyarova, G.A. Methyl Palmitate Hydrodeoxygenation over Silica-Supported Nickel Phosphide Catalysts in Flow Reactor: Experimental and Kinetic Study. *J. Chem. Technol. Biotechnol.* **2019**, *94*, 3007–3019. [CrossRef]
39. Kaewtrakulchai, N.; Smuthkochorn, A.; Manatura, K.; Panomsuwan, G.; Fuji, M.; Eiad-Ua, A. Porous Biochar Supported Transition Metal Phosphide Catalysts for Hydrocracking of Palm Oil to Bio-Jet Fuel. *Materials* **2022**, *15*, 6584. [CrossRef]
40. Shi, H.; Chen, J.; Yang, Y.; Tian, S. Catalytic Deoxygenation of Methyl Laurate as a Model Compound to Hydrocarbons on Nickel Phosphide Catalysts: Remarkable Support Effect. *Fuel Process. Technol.* **2014**, *118*, 161–170. [CrossRef]
41. Zhao, S.; Li, M.; Chu, Y.; Chen, J. Hydroconversion of Methyl Laurate as a Model Compound to Hydrocarbons on Bifunctional Ni2P/SAPO-11: Simultaneous Comparison with the Performance of Ni/SAPO-11. *Energy Fuels* **2014**, *28*, 7122–7132. [CrossRef]
42. Liu, C.; Yang, H.; Jing, Z.; Xi, K.; Qiao, C. Hydrodeoxygenation of Fatty Acid Methyl Esters and Isomerization of Products over NiP/SAPO-11 Catalysts. *J. Fuel Chem. Technol.* **2016**, *44*, 1211–1216. [CrossRef]
43. Tian, S.; Chen, J. Hydroisomerization of N-Dodecane on a New Kind of Bifunctional Catalyst: Nickel Phosphide Supported on SAPO-11 Molecular Sieve. *Fuel Process. Technol.* **2014**, *122*, 120–128. [CrossRef]
44. Liu, S.; Zhu, Q.; Guan, Q.; He, L.; Li, W. Bio-Aviation Fuel Production from Hydroprocessing Castor Oil Promoted by the Nickel-Based Bifunctional Catalysts. *Bioresour. Technol.* **2015**, *183*, 93–100. [CrossRef]
45. Tang, H.; Lin, J.; Cao, Y.; Jibran, K.; Li, J. Influence of NiMoP Phase on Hydrodeoxygenation Pathways of Jatropha Oil. *Energy* **2022**, *243*, 123048. [CrossRef]
46. Zhang, Y.; Wang, W.; Jiang, X.; Su, X.; Kikhtyanin, O.V.; Wu, W. Hydroisomerization of N-Hexadecane over a Pd–Ni2P/SAPO-31 Bifunctional Catalyst: Synergistic Effects of Bimetallic Active Sites. *Catal. Sci. Technol.* **2018**, *8*, 817–828. [CrossRef]
47. Wang, J.; Wang, Y.; Chen, G.; He, Z. Highly Loaded and Dispersed Ni2P/Al2O3 Catalyst with High Selectivity for Hydrogenation of Acetophenone. *Catalysts* **2018**, *8*, 309. [CrossRef]
48. Shamanaev, I.V.; Deliy, I.V.; Gerasimov, E.Y.; Pakharukova, V.P.; Kodenev, E.G.; Aleksandrov, P.V.; Bukhtiyarova, G.A. Synergetic Effect of Ni2P/SiO2 and γ-Al2O3 Physical Mixture in Hydrodeoxygenation of Methyl Palmitate. *Catalysts* **2017**, *7*, 329. [CrossRef]
49. Shamanaev, I.V.; Suvorova, A.O.; Gerasimov, E.Y.; Pakharukova, V.P.; Panafidin, M.A.; Yakovlev, I.V.; Bukhtiyarova, G.A. SRGO Hydrotreating over Ni-Phosphide Catalysts on Granulated Al2O3. *Catal. Today* **2021**, *378*, 24–32. [CrossRef]
50. Wang, Y.; Nuzhdin, A.L.; Shamanaev, I.V.; Kodenev, E.G.; Gerasimov, E.Y.; Bukhtiyarova, M.V.; Bukhtiyarova, G.A. Effect of Phosphorus Precursor, Reduction Temperature, and Support on the Catalytic Properties of Nickel Phosphide Catalysts in Continuous-Flow Reductive Amination of Ethyl Levulinate. *Int. J. Mol. Sci.* **2022**, *23*, 1106. [CrossRef]

51. Hasanudin, H.; Asri, W.R.; Andini, L.; Riyanti, F.; Mara, A.; Hadiah, F.; Fanani, Z. Enhanced Isopropyl Alcohol Conversion over Acidic Nickel Phosphate-Supported Zeolite Catalysts. *ACS Omega* **2022**, *7*, 38923–38932. [CrossRef] [PubMed]
52. Sheng, Q.; Li, X.; Prins, R.; Liu, C.; Hao, Q.; Chen, S. Understanding the Reduction of Transition-Metal Phosphates to Transition-Metal Phosphides by Combining Temperature-Programmed Reduction and Infrared Spectroscopy. *Angew. Chem. Int. Ed.* **2021**, *60*, 11180–11183. [CrossRef] [PubMed]
53. Shamanaev, I.V.; Deliy, I.V.; Pakharukova, V.P.; Gerasimov, E.Y.; Rogov, V.A.; Bukhtiyarova, G.A. Effect of the Preparation Conditions on the Physicochemical and Catalytic Properties of Ni_2P/SiO_2 Catalysts. *Russ. Chem. Bull.* **2015**, *64*, 2361–2370. [CrossRef]
54. Shin, M.; Kim, J.; Suh, Y.-W. Etherification of Biomass-Derived Furanyl Alcohols with Aliphatic Alcohols over Silica-Supported Nickel Phosphide Catalysts: Effect of Surplus P Species on the Acidity. *Appl. Catal. A Gen.* **2020**, *603*, 117763. [CrossRef]
55. Wang, Y.; Nuzhdin, A.L.; Shamanaev, I.V.; Bukhtiyarova, G.A. Flow Synthesis of N-Alkyl-5-Methyl-2-Pyrrolidones over Ni2P/SiO2 Catalyst. *Mol. Catal.* **2021**, *515*, 111884. [CrossRef]
56. Chen, J.; Shi, H.; Li, L.; Li, K. Deoxygenation of Methyl Laurate as a Model Compound to Hydrocarbons on Transition Metal Phosphide Catalysts. *Appl. Catal. B Environ.* **2014**, *144*, 870–884. [CrossRef]
57. Chen, J.; Han, M.; Zhao, S.; Pan, Z.; Zhang, Z. An in Situ Approach to Preparing Ni2P/SiO2 Catalyst under Mild Conditions and Its Performance for the Deoxygenation of Methyl Laurate to Hydrocarbons. *Catal. Sci. Technol.* **2016**, *6*, 3938–3949. [CrossRef]
58. Park, K.-C.; Ihm, S.-K. Comparison of Pt/Zeolite Catalysts for n-Hexadecane Hydroisomerization. *Appl. Catal. A Gen.* **2000**, *203*, 201–209. [CrossRef]